Landsat 9 Satellite Images Potentiality in Extracting Land Cover Classes in GEE Environment Using an Index-Based Approach: The Case Study of Savona City

Alessandra Capolupo(✉) and Eufemia Tarantino

Department of Civil, Environmental, Land, Building Engineering and Chemistry (DICATECh), Politecnico di Bari, Via Orabona 4, 70125 Bari, Italy
alessandra.capolupo@poliba.it

Abstract. Land use and land cover modeling is an essential tool because it enables scientists and policymakers to foresee prospective changes in landscape heritage and examine trends to minimize potential dangers. To attain this purpose, a continuous stream of data needs be collected and examined. Landsat missions present a viable alternative since they have been collecting continuous data for five decades, and a new platform was launched at the end of September 2021 to avoid disrupting such a series. Consequently, the purpose of this research is to assess the quality of Landsat 9 data in extracting land use information using the index-based approach. Following the conclusion of the collection and pre-processing operations, two of the most often used vegetation indices, NDVI and MSAVI2, were derived from a Landsat 9 data covering Savona city, which was chosen as the pilot site due to its unique geomorphological characteristics. Lastly, maps accuracy was assessed by computing the confusion matrices, k estimator and overall, producer and users accuracy. The entire method was implemented in the free cloud computing platform Google Earth Engine by writing custom Java code. The generated land use/cover maps were both satisfactory, albeit the MSAVI2 had a greater overall accuracy (90.24% vs 79.60%) and K parameter (84.45% vs 71.70%) due to its ability to minimize soil spectral effect. Those findings are consistent with those derived from Landsat 8 images. This means that Landsat 9 is an excellent successor to Landsat 8.

Keywords: satellite open images · geospatial big data · land use classification algorithms · cloud computing · NDVI · MSAVI2

1 Introduction

Among Earth observation systems, the Landsat initiative stands out because it has gathered continuous data for five decades, allowing researchers to explore Earth's physical process laws and dynamic evolution despite its poor, or at least medium, resolution [1]. As a result, it appears to be ideal for conducting ecological analyses and detecting changes in Land Use/Cover (LU/LC) from the early 1970s [2–4] which is the primary

© The Author(s), under exclusive license to Springer Nature Switzerland AG 2023
O. Gervasi et al. (Eds.): ICCSA 2023 Workshops, LNCS 14107, pp. 251–265, 2023.
https://doi.org/10.1007/978-3-031-37114-1_17

cause of significant environmental crises such as climate change or erosion [5–7]. Therefore, having incessant and accurate LU/LC maps looks to be critical in addressing the primary environmental challenges.

To ensure that data gathering does not cease, a new Landsat satellite mission, Landsat 9, was launched at the end of September 2021 by the National Aeronautics and Space Adminstration (NASA) and the US Geological Survey (USGS). To enhance observational timing, it was sent into orbit eight days following Landsat 8, guaranteeing the acquisition of around 1,500 new scenes every day [6]. Indeed, the geometric, temporal, and spectral resolutions of the Landsat 8 OLI sensor and the Landsat 9 OLI-2 sensor are nearly identical. The key distinction between them is the greater radiometric resolution (14 bits) of the Landsat 9 sensor against the OLI sensor's 12-bit resolution [9].

Landsat missions therefore provide an essential baseline data set, however only few images are truly helpful because the majority of them are impacted by climatic circumstances and, as a result, cannot be used to give relevant information [10]. Furthermore, two additional issues must be addressed: i) the vast number of data to be processed to meet a specific purpose, and ii) the detection of the best technique to extract LU/LC information in a short period of time. The former issue might be addressed by utilizing a web-based platform designed to manage geographical large data, such as Google Earth Engine (GEE - https://earthengine.google.org) [11]. The latter, on the other hand, might be addressed by assessing the many algorithms produced over time and picking the best one in accordance with the study goal.

GEE, in fact, allows users to review the integrated data catalogue, which is updated daily, and choose one of the actual accessible open-source geospatial data or import a proprietary layer to process in the Application Programming Interface (API) [12]. API enables to manage hundreds of geographical data at the same time by writing appropriate codes in Java or Python languages and making use of the collection of complex algorithms already integrated in such a platform [11]. As a consequence, any user has the ability to write their own code or customize existing ones. Also, each algorithm is sped up due to the number of processors engaged throughout the running phase. This even eliminates any challenges related with the storage, management, and analysis of massive volumes of geographical big data, going beyond the constraints of the frequently applied desktop software. Although they feature a smart, interactive, and user-friendly interface that can be utilized by both IT-skilled and non-IT-skilled people [13–15], in most cases, such software are black boxes, as they do not disclose any understanding about the adopted procedures. Because they are not flexible, only pre-existing algorithms may be used to process the data and, then, the optimal processing approach may not be available [16].

In fact, numerous ways to dealing with geographic big data and creating LU/LC maps have been created throughout the years. The most recurrent ones are index-based [17, 18], machine learning (ML) [19–21], and Object-Based Image Analysis (OBIA) [22, 23]. So far, none of them are without restrictions. In fact, the index-based technique can only extract information from one LU/LC category, whereas ML requires a large number of parameters that are difficult to implement, and OBIA does not deliver promising results on low/medium resolution images [24–27]. As a result, it is critical to select the optimal strategy based on the input data and study objectives.

In this research, the index-based approach was used to generate LU/LC maps from satellite images quickly. This decision was made to assess the potential of the new satellite platform Landsat 9. Furthermore, while it delivers data in continuity with Landsat 8, its potential has yet to be tapped since it is so new. Furthermore, the free cloud computing GEE platform was used to speed up the operation and customize the categorization algorithms based on study needs. The approach was tried at a pilot site in Savona, a town in the Liguria area of northern Italy, selected because of its morphological complexity.

The paper is structured as follows: Part 2 "Materials and Methods" explains the city of Savona, the chosen pilot site where the technique was evaluated (Sect. 2.1), as well as the methodology used to generate the geodatabase in the GEE environment (Sect. 2.2) and to handle Landsat 9 satellite pictures (Sects. 2.2 and 2.3). Finally, the process for determining the accuracy of the resultant maps is evaluated (Sect. 2.4). Part 3 "Results and discussion" presents and discusses the final results relating to the generating LU/LC maps, map accuracy, Landsat 9 image quality, and script performance. The Conclusion section highlights more improvements and criticality.

2 Material and Methods

This section displays the techniques used to attain the study objectives. Indeed, after consulting GEE catalogue and collecting the input Landsat 9 images, they were preprocessed to rectify the atmospheric conditions and remove cloud cover (Sect. 2.2). The pansharpenig technique was also applied to increase their spatial resolution. Following that, the index-based classification method was used to extract land use information by implementing two indices, NDVI and MSAVI2 (Sect. 2.3). The accuracy metrics, such as Overall Accuracy (OA), Producer Accuracy (PA), User Accuracy (UA), and Kappa coefficient (K) were used to estimate the reliability of the resulting classification maps (Sect. 2.4). Finally, the performance of the two indices derived from Landsat 9 images is discussed. All steps were finalized by writing appropriate code in the open-source GEE environment.

2.1 Study Area

Savona city, in Liguria region, is situated on a tiny alluvial plain produced by the Letimbro River on the Riviera di Ponente (Fig. 1). It includes a large patch of the upper basin of the Bormida from the shore to the Alpine-Appennine lake. It is mostly hilly, and it contains the Colle di Cadibona, which connects the Alps to the Appennino. The main watercourse is the Centa, which runs through Albenga.

Throughout the twentieth century, the population grew along the coast, both north and south, until it reached Vado Ligure and Albisola Marina, and it absorbed other minor towns, resulting in a conurbation of around 115,000 people. The old town, which is located between the port and the ancient fortress, is a maze of tiny and twisting alleys studded with piazzas and elegant homes (Priamar). Newer communities, on the other hand, feature a tiered plant with broad, straight roadways.

The port is the economic core of the metropolitan area, allowing the city to fulfill key economic duties since its establishment, and it is served by 18-km funicular railways

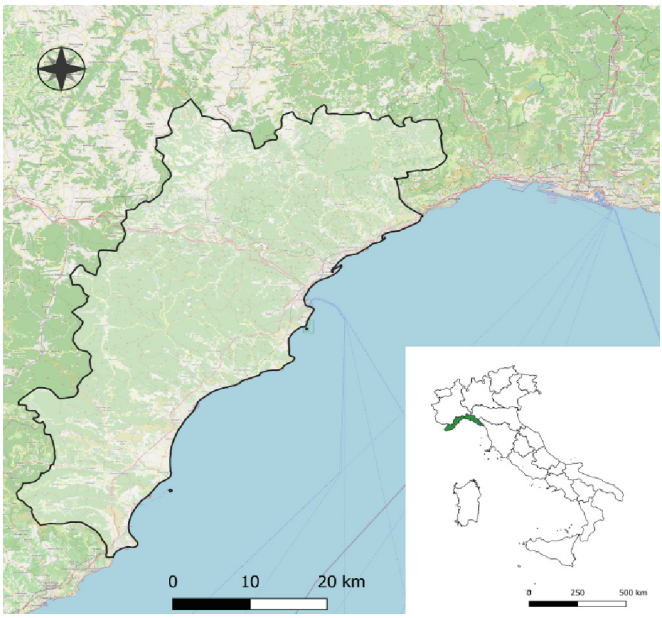


Fig. 1. The study area's location. On the bottom is an overview of the Italian context, with the Liguria Region highlighted in green, and on the top, the administrative boundaries of Savona are represented on the freely available Open Street Map (OSM) service.

designed to transfer carbon from the mountains to the city. In the 1960s, the convergence of vital freight rivers at Genoa's nearby massive port drove Savona to focus on the export of specialized products, namely petroleum. Following that, Savona's port underwent a series of transformations, resulting in a gradual shift of industrial port activities to the area of Vado Ligure, while the city seaport, which has been completely redesigned in terms of infrastructure, has emphasized its touristic vocation, focusing particularly on passenger traffic. In fact, tourism, along with the agricultural and industrial sectors, is vital to the local economy.

2.2 Database Construction and Preprocessing Step

Google created and launched GEE, a new cloud platform for storing and processing geospatial big data in 2017 [11]. It is made up of three major components: a high-performance computing (HPC) infrastructure, a large number of processors dedicated to speeding up the procedure and running custom-designed algorithms, and, lastly, a data catalogue that is updated daily with approximately 6000 freely available scenes collected by active missions and Digital Elevation Models (DEMs) with various resolution as well as vector, topographic and climate data [12]. Such data can be downloaded in both raw and pre-processed formats for use with desktop software, or they may be directly uploaded into the GEE API [28, 29]. In this case, the second option was picked. After reviewing the catalogue, indeed, the most suited Landsat 9 satellite images covering the research location were imported into GEE API. Apart from the satellite mission and pilot

site location, cloud cover information was also taken into account: only scenes with a cloud cover value of less than 30% were examined. In contrast, any acquisition time constraint was not imposed due to the scarcity of Landsat data; the satellite mission was launched by the end of September 2021. Finally, only Level-2 data were examined.

Thus, after importing into the API an image collection acquired from Landsat 9 mission from November 2021 up to November 2022 and filtering the images based on the aforementioned cloud cover and level information, just one image, dated January 2022 and having a cloud cover percentage of 10%, was satisfactory and selected to be processed in the further steps. That image was given in the Universal Transverse Mercator projection and the World Geodetic System (WGS84) datum. At this stage, a cloud masking procedure was performed, which required employing suitable filters to make the clouds invisible and omitting the corresponding pixels throughout the processing phase [30, 31]. Mateo Garcia's approach [32] based on information provided by the quality assessment band was used to attain this purpose. In contrast, no further orthorectification phase was necessary since the accuracy of the process was deemed enough, and a pansharpening approach was applied to increase picture resolution using the algorithm established by Stuhler et al., (2016) [33] for handling Landsat 8 images. "Pansharpening" is the final stage of the pre-processing technique. This means that the generated image served as the categorization procedure's input data. Figure 2 depicts the entire pre-processing operation.

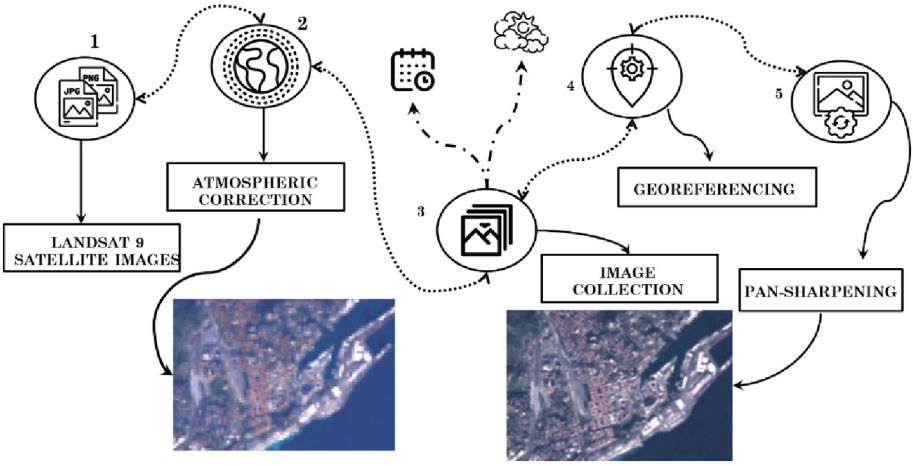


Fig. 2. Preprocessing workflow

2.3 Index-Based Classification Approach

The corrected image was then used as input data in the index-based classification method. An approach like this is useful for quickly separating LU/LC classes from satellite data [34]. This attribute makes this approach more appealing than any other classification strategies when a large number of data or a large region must be investigated. As a

consequence, an enormous number of indexes that can extract Earth's characteristics based on their spectral signature have been devised. Because each object's spectral signature indicates its ability to absorb, reflect, and transmit energy, items in the same LU/LC class do not have the same trend, but rather a comparable one. Because each object's spectral signature indicates elements' ability to absorb, reflect, and transmit energy, items in the same LU/LC class do not have the same signature trend, but rather a comparable one. As a result, each index entails the incorporation of distinct bands capable of evaluating a certain LU/LC category. Red and Red Edge bands, for example, are often used to detect green regions and water [35], whereas TIR and SWIR bands are commonly utilized to identify bare soil [36] and built-up areas [37], as well as to extract information about sparse and thick vegetation [38]. Thus, only few indicators are appropriate for classifying an entire area [39]. In most circumstances, additional indexes must be merged to achieve this goal [40].

In this study, the performance of two vegetation indices, Normalized Difference Vegetation Index (NDVI) (Eq. 1) [41] and Modified Soil Adjusted Vegetation Index 2 (MSAVI2) (Eq. 2) [42], derived from Landsat 9, was test to classify the whole pilot site.

$$NDVI = \frac{\text{NIR} - \text{RED}}{NIR + RED} \tag{1}$$

$$\text{MSAVI2} = \frac{(2 * \text{NIR} + 1 - \sqrt{(2 * NIR + 1)^2 - 8 * (NIR - RED)}}{2} \tag{2}$$

As shown in Eqs. 1–2, NDVI and MSAVI2 integrate the same bands albeit in a different way. This indicates that they are both committed to identifying vegetated regions, but from distinct perspectives. Indeed, the former, which is primarily related to biomass development and plant health, is frequently used to assess vegetation phenology [43], whereas the latter is more suited when green zone are discontinuous due to its capacity to minimize soil spectral influence [42]. This means they give complimentary information and are frequently used to assess green space density and health condition [44]. Moreover, both indices are between -1 and + 1, with greater values increasing as the biomass concentration of the pixel rises. The accuracy of both maps, which is described in further detail in the next Section, was statistically determined.

2.4 Accuracy Assessment

The reliability of the resulting LULC classification maps was estimated, as indicated in [45, 46], by constructing a reference dataset with a number of testing samples proportionate to the class size. The stratified random sample point approach was utilized to produce such a data collection, and each generated sample was then manually examined and labeled according to its placement. The baseline land use information used to establish point position were produced by interpreting the satellite images overlaid on testing samples. This technique was iteratively repeated for all of the testing samples on each classified map. Based on these findings, Eqs. 3–6 were used to calculate accuracy metrics such as OA, PA, UA, and K [47, 48].

$$OA = \frac{\sum n_i}{N_{TOT}} \tag{3}$$

$$UA = \frac{n_{ii}}{n_{i+}} \tag{4}$$

$$PA = \frac{n_{ii}}{n_{+i}} \tag{5}$$

$$K = \frac{N_{TOT} \sum n_{ii} - \sum n_{iR} * n_{Pi}}{{N_{TOT}}^2 - \sum n_{iR} * n_{Pi}} \tag{6}$$

where N_{TOT} and n_i are the amount of correctly classified testing samples and the total number of testing samples, respectively. On the other hand, n_{ii} and n_{i+} represent the number of correctly identified testing samples belonging to a certain class and the number of reference samples comprising in such a category. Lastly, n_{iR} and n_{Pi} are the number of samples utilized in the test and classification classes, respectively. All parameters of the confusion matrix have a value between 0 and 1. The greater their worth, the greater the accuracy.

3 Results and Discussion

This research examined the ability of the newly developed Landsat 9 platform to extract LU/LC classes using an index-based method in GEE platform. As previously stated, while no classification technique is flawless in every situation, the index-based approach provides an efficient and resilient solution for automatically classifying the whole study area in a short period of time [49]. As a result, it was chosen as the standard for measuring the performance of the new satellite images. Thus, two distinct indices, NDVI [41] (Eq. 1) and MSAVI 2 [42] (Eq. 2), were calculated on a satellite image collected by Lansat 9 platform which was selected by consulting the GEE catalogue and imported in the API. To choose the most suitable data for the research, three primary criteria were established: i) Landsat mission, ii) a cloud cover percentage of less than 30%, and iii) a 2-level satellite data. In contrast, no assumptions were made regarding the acquisition date because the platform was newly started, and so just a few data are available. Also, most of them are ineffective due to climatic circumstances, therefore just one image, dated January 2022, was picked. Before to processing, its resolution was increased using the pan-sharpening technique (Fig. 2). The outcome was the input data for the index-based technique, the results of which are shown in Fig. 3.

Both indices distinguished four LU/LC categories: water, built-up areas, sparse and dense vegetation. Nevertheless, no significant difference was identified in water and built-up regions, represented by blue and red pixels, respectively. In contrast, the same quantity of green areas was found, even though the distribution of sparse and dense vegetation is radically different. In fact, the amount of sparse vegetation is greater than the amount of dense vegetation in MSAVI2, whereas the situation is exactly opposite in the NDVI map. This conclusion, which is obvious in Fig. 3, is accentuated in Fig. 4, where the distribution of LU/LC pixels is displayed in histogram charts. In both representations, the pixels devoted to water and built-up regions are same, as opposed to sparse and thick vegetation. This is due mostly to the disparity in information offered by the two indexes. These are vegetation indices established to differentiate green regions from

others, however as mentioned by [44], they are often employed in different scenarios. The former, NDVI, is more suited to characterize plant phenology since it is linked to biomass and plant health status, whereas MSAVI2 is better suited for neutralizing the influence of soil spectral signature. When the green patches are discontinuous, MSVAI2 accuracy outperforms NDVI.

This statement is also supported by the NDVI and MSAVI2 confusion matrices reported in Tables 1 and 4, respectively. Indeed, the detection of water and built-up areas is fairly accurate in both generated maps, whereas the distinction between sparse and dense vegetation is more accurate in the MSAVI2 chart. This means that NDVI is excellent at predicting vegetation but not at differentiating the density of green areas. Such an issue affects their OA and K value, despite the fact that both indicators show a promising result. Indeed, the NDVI and MSAVI2 OA values are 79.60% and 90.24%, respectively, while the K values are 71.70% and 84.45%. K is a measure of inter-rater reliability that takes a value between −1 and 1: the higher the value, the more reliable the results are. Thus, NDVI is consistent, whereas MSAVI2 is extremely trustworthy.

In general, the classes have high accuracy values from both the PA and the CA perspectives (Tables 2, 3, 5 and 6), but there are some important differences to consider. MSAVI2 provides minor accuracy values for the UA (68,46% vs 75.24%) in the urbanization class. This means that, even though 78.76% (PA) of urban areas are correctly classified, only 68.46% are truly urban. In contrast, NDVI shows a lot of misclassifications in sparse vegetation category. The UA is approximately equivalent to 47%, while the PA is about 50%. This is because most sparse green pixels are mislabeled as built-up or dense vegetation, and dense vegetation is misidentified as sparse green areas, as is evident from Table 1.

These observations are consistent with previous research findings in terms of accuracy and LU/LC classes isolated. According to Capolupo et al., (2020) [39], who evaluated classification indices on the pilot site of Margherita di Savoia (Puglia region) with similar morphological features, both indices are capable of extracting the four categories identified in this study plus bare soil. Their OA, however, were 73.24% and 83.30%, respectively.

Moreover, to speed up the procedure, GEE cloud computing platform was used through the development of an own code in Java language. Indeed, thanks to its parallel processors, such a script ran quickly, overcoming common desktop software constraints. Furthermore, the developed code can be easily applied to other case studies by simply adjusting the indices thresholds to the site surface features. As a result, GEE appears to be the best solution for processing geospatial big data quickly and customizing the algorithms to research specific needs.

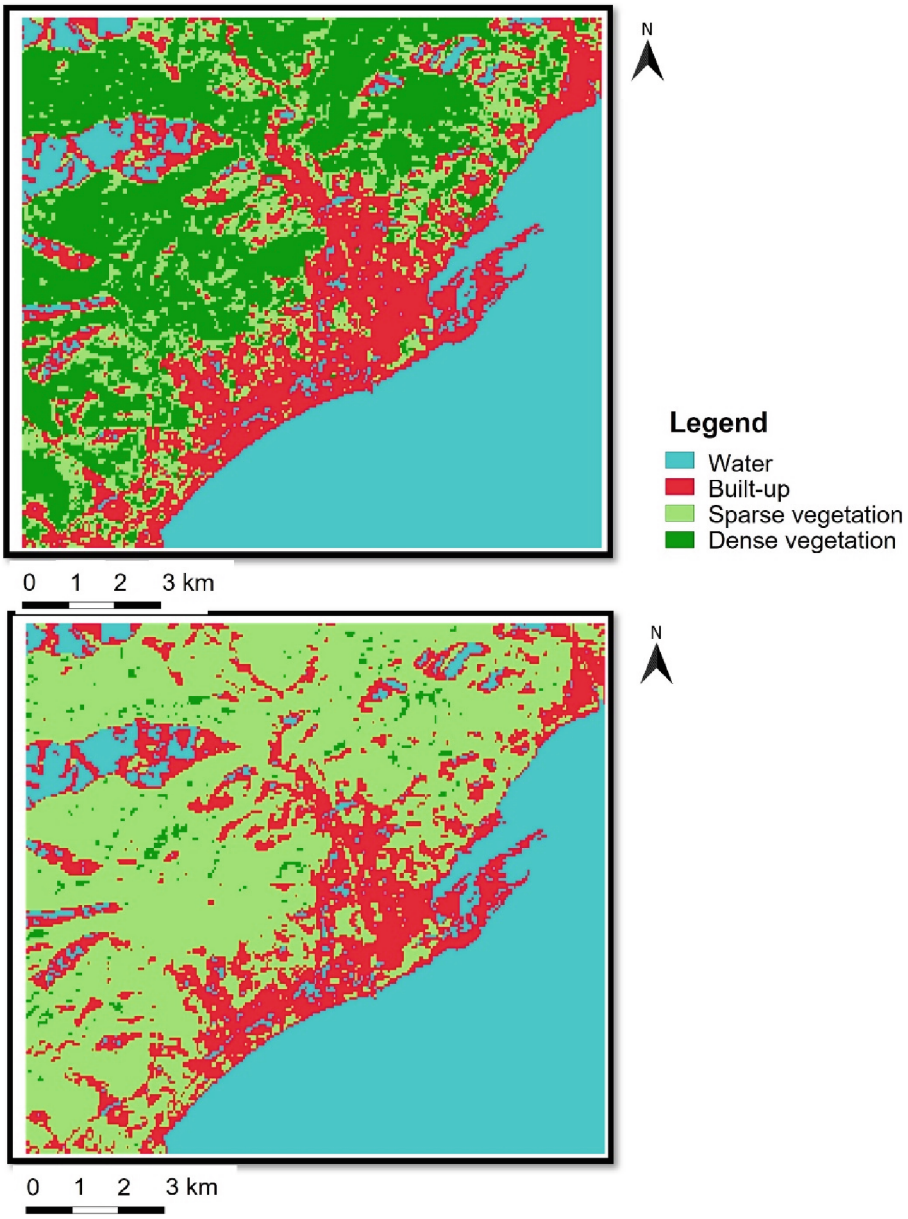


Fig. 3. Land cover maps created by calculating the NDVI (on the top) and MSAVI2 (on the bottom) indices using Landsat 9 images collected in January 2022.

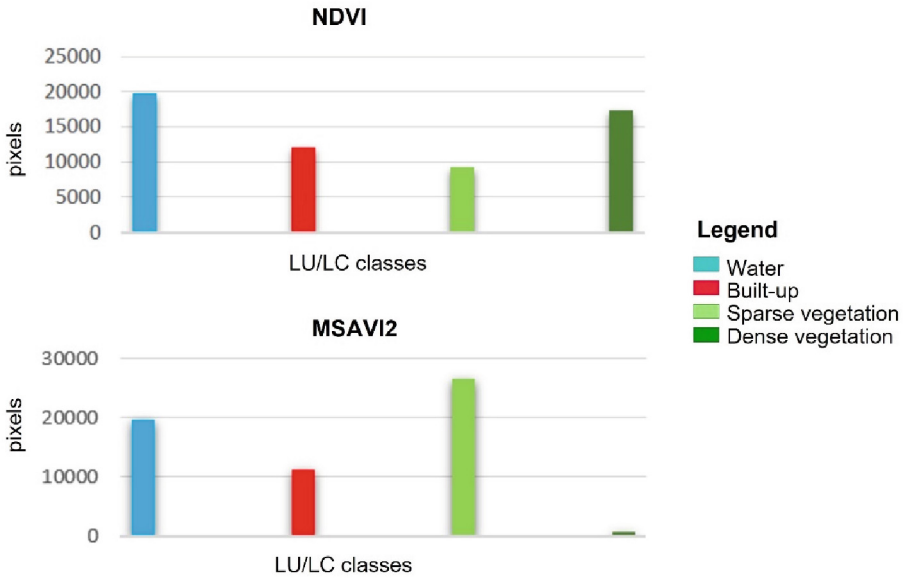


Fig. 4. Histograms of LU/LC classes

Table 1. Error matrix generated by computing NDVI on Landsat 9 image.

NDVI					
	Water	Built-up	Sparse Vegetation	Dense Vegetation	Tot
Water	257	12	2	1	272
Built-up	14	103	14	5	136
Sparse Vegetation	1	23	55	38	117
Dense Vegetation	0	4	39	182	225
Tot	272	142	110	226	750

Table 2. Producer Accuracy (PA) generated by computing NDVI on Landsat 9 image.

	PA		
Water	257/272	0.9449	94.49%
Built-up	103/142	0.7254	72.54%
Sparse Vegetation	55/110	0.5000	50.00%
Dense Vegetation	182/226	0.8053	80.53%

Table 3. User Accuracy (UA) generated by computing NDVI on Landsat 9 image.

	UA		
Water	257/272	0.9449	94.49%
Built-up	103/136	0.7574	75.74%
Sparse Vegetation	55/117	0.4701	47.01%
Dense Vegetation	182/225	0.8089	80.89%

Table 4. Confusion matrix generated by computing MSAVI2 on Landsat 9 image.

MSAVI2					
	Water	*Built-up*	*Sparse Vegetation*	*Dense Vegetation*	*Tot*
Water	249	11	1	0	261
Built-up	15	89	26	0	130
Sparse Vegetation	1	13	322	2	338
Dense Vegetation	0	0	3	6	9
Tot	265	113	352	8	738

Table 5. Producer Accuracy (PA) generated by computing MSAVI2 on Landsat 9 image.

	PA		
Water	249/265	0.9496	93.96%
Built-up	89/113	0.7976	78.76%
Sparse Vegetation	322/352	0.9148	91.48%
Dense Vegetation	6/8	0.7500	75.00%

Table 6. User Accuracy (UA) generated by computing MSAVI2 on Landsat 9 image.

	UA		
Water	249/261	0.9540	95.40%
Built-up	89/130	0.6846	68.46%
Sparse Vegetation	322/338	0.9527	95.27%
Dense Vegetation	6/9	0.6667	66.67%

4 Conclusion

The purpose of this study was to evaluate the feasibility of the index-based approach for extracting LU/LC classes from new optical satellite images given by NASA/USGS: Landsat 9 data. As a result, two of the most often used indicators for retrieving information about the health status and distribution of green spaces were evaluated on the pilot site of Savona city, which was chosen for its specific morphological features, NDVI and MSAVI2. Because of its relationship with biomass, the former is typically used to measure plant phenology, whilst the latter is particular for reducing background soil influence. Although both indices have been shown to be strong predictors of vegetated pixels, MSAVI2 exhibited greater OA and K values in identifying water and sparse and thick vegetation. As a result, it looks to be better suited to investigating green area conditions using medium-resolution satellite data.

Furthermore, by comparing their results to those of earlier studies that used similar indices on Landsat 8 images, it is clear that their results are consistent. Hence, despite the fact that Landsat 9 has higher radiometric resolution, the results obtained did not vary from those obtained with Lansat 8. These observations developed for the research area have the potential to be transferred to other places without any variations. Finally, using the GEE platform allows customers to automate and speed up the entire process, lowering both data collecting and processing time.

References

1. Belward, A.S., Skøien, J.O.: Who launched what, when and why; trends in global land-cover observation capacity from civilian earth observation satellites. ISPRS J. Photogramm. Remote. Sens. **103**, 115–128 (2015)
2. Goward, S.N., Williams, D.L.: Landsat and earth systems science: development of terrestrial monitoring. Photogramm. Eng. Remote Sens. **63**(7), 887–900 (1997)
3. Zhu, Z., et al.: Benefits of the free and open Landsat data policy. Remote Sens. Environ. **224**, 382–385 (2019)
4. Mbow, H.O.P., Reisinger, A., Canadell, J., O'Brien, P.: Special Report on climate change, desertification, land degradation, sustainable land management, food security, and greenhouse gas fluxes in terrestrial ecosystems (SR2). Ginevra, IPCC, vol. 650 (2017)
5. Capolupo, A., Saponaro, M., Fratino, U., Tarantino, E.: Detection of spatio-temporal changes of vegetation in coastal areas subjected to soil erosion issue. Aquat. Ecosyst. Health Manag. **23**(4), 491–499 (2020)
6. Boccia, L., Capolupo, A., Rigillo, M., Russo, V.: Terrace abandonment hazards in a Mediterranean cultural landscape. J. Hazard. Tox. Radioact. Waste **24**(1), 04019034 (2020)
7. Capolupo, A., Boccia, L.: Innovative method for linking anthropisation process to vulnerability. World Rev. Sci. Technol. Sustain. Dev. **17**(1), 4–22 (2021)
8. Lulla, K., Nellis, M.D., Rundquist, B., Srivastava, P.K., Szabo, S.: Mission to earth: LANDSAT 9 will continue to view the world. Geocarto Int. **36**(20), 2261–2263 (2021)
9. Masek, J.G., et al.: Landsat 9: Empowering open science and applications through continuity. Remote Sens. Environ. **248**, 111968 (2020)
10. Potapov, P., Turubanova, S., Hansen, M.C.: Regional-scale boreal forest cover and change mapping using Landsat data composites for European Russia. Remote Sens. Environ. **115**(2), 548–561 (2011)

11. Gorelick, N., Hancher, M., Dixon, M., Ilyushchenko, S., Thau, D., Moore, R.: Google Earth Engine: Planetary-scale geospatial analysis for everyone. Remote Sens. Environ. **202**, 18–27 (2017)
12. Kumar, L., Mutanga, O.: Google earth engine applications since inception: usage, trends, and potential. Remote Sens. **10**, 1509 (2018)
13. Capolupo, A., et al.: An interactive WebGIS framework for coastal erosion risk management. J. Mar. Sci. Eng. **9**(6), 567 (2021)
14. Capolupo, A., Monterisi, C., Tarantino, E.: Development of an open-source 3D WebGIS framework to promote cultural heritage dissemination. in extended reality. In: De Paolis, L.T., Arpaia, P., Sacco, M. (eds.) First International Conference, XR Salento 2022, Lecce, Italy, 6–8 July 2022, Proceedings, Part II, pp. 254–268. Springer, Cham (2022). https://doi.org/10.1007/978-3-031-15553-6_19
15. Capolupo, A., et al.: Workshops: Malaga, Spain, July 4–7, 2022, Proceedings, Part III, pp. 340–353. Springer International Publishing, Cham (2022)
16. Steiniger, S., Hunter, A.J.: Free and open source GIS software for building a spatial data infrastructure. In: OGRS, pp. 247–261 (2009)
17. Chen, Y., Gong, P.: Clustering based on eigenspace transformation–CBEST for efficient classification. ISPRS J. Photogramm. Remote. Sens. **83**, 64–80 (2013)
18. Matsushita, B., Yang, W., Chen, J., Onda, Y., Qiu, G.: Sensitivity of the enhanced vegetation index (EVI) and normalized difference vegetation index (NDVI) to topographic effects: a case study in high-density cypress forest. Sensors **7**(11), 2636–2651 (2007)
19. Abdi, A.M.: Land cover and land use classification performance of machine learning algorithms in a boreal landscape using Sentinel-2 data. GIScience Remote Sens. **57**(1), 1–20 (2020)
20. Ladisa, C., Capolupo, A., Ripa, M.N., Tarantino, E.: Combining OBIA approach and machine learning algorithm to extract photovoltaic panels from Sentinel-2 images automatically. In: Remote Sensing for Agriculture, Ecosystems, and Hydrology XXIV, vol. 12262, pp. 67–76. SPIE (2022)
21. Tarantino, E., Novelli, A., Aquilino, M., Figorito, B., Fratino, U.: Comparing the MLC and JavaNNS approaches in classifying multi-temporal LANDSAT satellite imagery over an ephemeral river area. Int. J. Agric. Environ. Inf. Syst. (IJAEIS) **6**(4), 83–102 (2015)
22. Crocetto, N., Tarantino, E.: A class-oriented strategy for features extraction from multidate ASTER imagery. Remote Sens. **1**(4), 1171–1189 (2009)
23. Novelli, A., Aguilar, M.A., Nemmaoui, A., Aguilar, F.J., Tarantino, E.: Performance evaluation of object based greenhouse detection from Sentinel-2 MSI and Landsat 8 OLI data: A case study from Almería (Spain). Int. J. Appl. Earth Obs. Geoinf. **52**, 403–411 (2016)
24. Breiman, L.: Random forests. Machine learning **45**, 5–32 (2001)
25. Homer, C., Huang, C., Yang, L., Wylie, B.K., Coan, M.: Development of a 2001 national land-cover database for the United States (2004)
26. Anchang, J.Y., Ananga, E.O., Pu, R.: An efficient unsupervised index based approach for mapping urban vegetation from IKONOS imagery. Int. J. Appl. Earth Obs. Geoinf. **50**, 211–220 (2016)
27. Figorito, B., Tarantino, E., Balacco, G., Fratino, U.: An object-based method for mapping ephemeral river areas from WorldView-2 satellite data. In: Remote Sensing for Agriculture, Ecosystems, and Hydrology XIV, vol. 8531, pp. 68–76. SPIE (2012)
28. Capolupo, A., Monterisi, C., Saponaro, M., Tarantino, E.: Multi-temporal analysis of land cover changes using Landsat data through Google Earth Engine platform. In: Eighth International Conference on Remote Sensing and Geoinformation of the Environment (RSCy2020), vol. 11524, pp. 447–458. SPIE (2020)

29. Sangiorgio, V., Capolupo, A., Tarantino, E., Fiorito, F., Santamouris, M.: Evaluation of absolute maximum urban heat island intensity based on a simplified remote sensing approach. Environ. Eng. Sci. **39**(3), 296–307 (2022)
30. Caprioli, M., Figorito, B., Tarantino, E.: Radiometric normalization of Landsat ETM+ data for multitemporal analysis. In: Proceedings of ISPRS Commission VII Mid-Term Symposium on "Remote Sensing: from Pixels to Processes", Enschede (unpaginated CD-ROM) (2006)
31. Tarantino, E., Figorito, B., Caprioli, M.: Comparison of radiometric normalization methods on LANDSAT ETM+ and ASTER data. Bollettino di Geodesia e Scienze Affini **67**(2), 89–106 (2008)
32. Mateo-García, G., Gómez-Chova, L., Amorós-López, J., Muñoz-Marí, J., Camps-Valls, G.: Multitemporal cloud masking in the Google Earth Engine. Remote Sens. **10**, 1079 (2018)
33. Stuhler, S. C., Leiterer, R., Joerg, P. C., Wulf, H., Schaepman, M.E.: Generating a cloud-free, homogeneous Landsat-8 mosaic of Switzerland using Google Earth Engine (2016)
34. Patel, N.N., Angiuli, E., et al.: Multitemporal settlement and population mapping from Landsat using Google Earth Engine. Int. J. Appl. Earth Obs. Geoinf. **35**, 199–208 (2015)
35. Capolupo, A., Kooistra, L., Berendonk, C., Boccia, L., Suomalainen, J.: Estimating plant traits of grasslands from UAV-acquired hyperspectral images: a comparison of statistical approaches. ISPRS Int. J. Geo Inf. **4**(4), 2792–2820 (2015)
36. Kazakis, N., Kougias, I., Patsialis, T.: Assessment of flood hazard areas at a regional scale using an index-based approach and analytical hierarchy process: application in Rhodope-Evros region, Greece. Sci. Total Environ. **538**, 555–563 (2015)
37. Southworth, J.: An assessment of Landsat TM band 6 thermal data for analysing land cover in tropical dry forest regions. Int. J. Remote Sens. **25**(4), 689–706 (2004)
38. Yusuf, B.L., He, Y.: Application of hyperspectral imaging sensor to differentiate between the moisture and reflectance of healthy and infected tobacco leaves. Afr. J. Agric. Res **6**(29), 6267–6280 (2011)
39. Capolupo, A., Monterisi, C., Caporusso, G., Tarantino, E.: Extracting land cover data using GEE: a review of the classification indices. In: Gervasi, O., et al. (eds.) ICCSA 2020. LNCS, vol. 12252, pp. 782–796. Springer, Cham (2020). https://doi.org/10.1007/978-3-030-58811-3_56
40. Sarzana, T., Maltese, A., Capolupo, A., Tarantino, E.: Post-processing of pixel and object-based land cover classifications of very high spatial resolution images. In: Gervasi, O., et al. (eds.) ICCSA 2020. LNCS, vol. 12252, pp. 797–812. Springer, Cham (2020). https://doi.org/10.1007/978-3-030-58811-3_57
41. Rouse, J.W., Haas, R.H., Schell, J.A., Deering, D.W.: Monitoring vegetation systems in the Great Plains with ERTS. NASA Spec. Publ. **351**(1), 309 (1974)
42. Qi, J., Chehbouni, A., Huete, A.R., Kerr, Y.H., Sorooshian, S.: A modified soil adjusted vegetation index. Remote Sens. Environ. **48**(2), 119–126 (1994)
43. Bannari, A., Morin, D., Bonn, F., Huete, A.R.: A review of vegetation indices. Remote Sens. Rev. **13**, 95–120 (1995)
44. Borgogno-Mondino, E., de Palma, L., Novello, V.: Investigating Sentinel 2 multispectral imagery efficiency in describing spectral response of vineyards covered with plastic sheets. Agronomy **10**(12), 1909 (2020)
45. Sidhu, N., Pebesma, E., Câmara, G.: Using Google Earth Engine to detect land cover change: Singapore as a use case. Eur. J. Remote Sens. **51**, 486–500 (2018)
46. Pengra, B., Long, J., Dahal, D., Stehman, S.V., Loveland, T.R.: A global reference database from very high-resolution commercial satellite data and methodology for application to Landsat derived 30 m continuous field tree cover data. Remote Sens. Environ. **165**, 234–248 (2015)

47. Stehman, S.V.; Woodcock, C.E.; Sulla-Menashe, D.; Sibley, A.M.; Newell, J.D.; Friedl, M.A.; Herold, M. A global land-cover validation data set. part I: Fundamental design principles. Int. J. Remote Sens. 2012, 33, 5768–5788
48. Caprioli, M., Tarantino, E.: Accuracy assessment of per-field classification integrating very fine spatial resolution satellite imagery with topographic data. J. Geospat. Eng. **3**, 127–134 (2001)
49. Tarantino, E., Figorito, B.: Mapping rural areas with widespread plastic covered vineyards using true color aerial data. Remote Sens. **4**(7), 1913–1928 (2012)